Modulation Concepts for the Control of a Two-Phase Bearingless Slice Motor Utilizing Three-Phase Power Modules

M.T. Bartholet, T. Nussbaumer*, D. Krähenbühl, F. Zürcher, J.W. Kolar

Power Electronic Systems Laboratory
ETH Zurich
8092 Zurich, SWITZERLAND
bartholet@eek.ee.ethz.ch

*Levitronix GmbH
Technoparkstrasse 1
8005 Zurich Switzerland
nussbaumer@levitronix.com

***Abstract*—Future application areas for bearingless pump systems will demand for highly compact and cost effective designs. This trend mainly has a major impact on the power electronics part of these systems. Up to now, full-bridge converters have been used in order to independently control the phases of the active magnetic bearing and the drive system. With the use of an interleaved half-bridge topology the number of required power semiconductors is reduced by 25%. In this paper, novel modulation techniques are presented and comparatively evaluated in order to achieve a similar dynamic performance of the pump system as with the conventional full-bridge topology. The effects of a phase shift and of higher harmonics in the duty cycles are analyzed in detail. The proposed concepts are then implemented on a DSP board and their feasibility is shown on a highly compact 1.5 kW prototype of a converter which is realized with two integrated three-phase power modules. Furthermore, it is shown that the higher harmonics injection does not have an impact on the average speed of the impeller and thus on the constant output flow of the pump.**

I. INTRODUCTION

New application areas for bearingless pump systems such as electroplating, the food industry as well as in the area of the biotechnology [1] require the development of very compact and cost efficient converter designs for the bearingless slice motor (BSM) system [2]. The various benefits of the bearingless pump for the handling of very pure and aggressive fluids in the semiconductor industry and for medical applications are described in literature [3]. However, in order to attract new markets for the BSM-technology the whole system must become economically more attractive. Research so far has only been carried out on the motor itself and very little research effort has been focused on the investigation of novel topologies to control the drive and bearing system.

In a first approach, a novel topology for the control of the two-phase BSM system has been presented in [4] which decreases the number of required semiconductors by 25%. By connecting two drive/bearing windings to common bridge legs and utilizing three-phase power modules (cf. **Fig. 1**(b)), which are available off-the-shelf, a higher efficiency and a more compact design of the power electronics part can be achieved. Based on this, different modulation schemes for the control of the pump with the interleaved half bridge topology are investigated and comparatively evaluated in this paper.

The BSM utilized in this paper has a symmetrical winding configuration with two bearing phases L_{B1} and L_{B2} and two drive phases L_{D1} and L_{D2} as it is depicted in **Fig. 2**. The stabilisation of the rotor is realised with contactless magnetic bearings that are placed around eight claws which are carrying the flux of the bearing and drive system. The control of the current in each drive and bearing winding, and thus the flux, is up to now performed by one separate full-bridge converter for each phase. This results in a total number of sixteen power transistor/diode combinations for the converter (cf. Fig. 1(a)). The orthogonal placement of the coils in the motor yields a $\pi/2$ phase shift of the currents in the drive windings under operation.

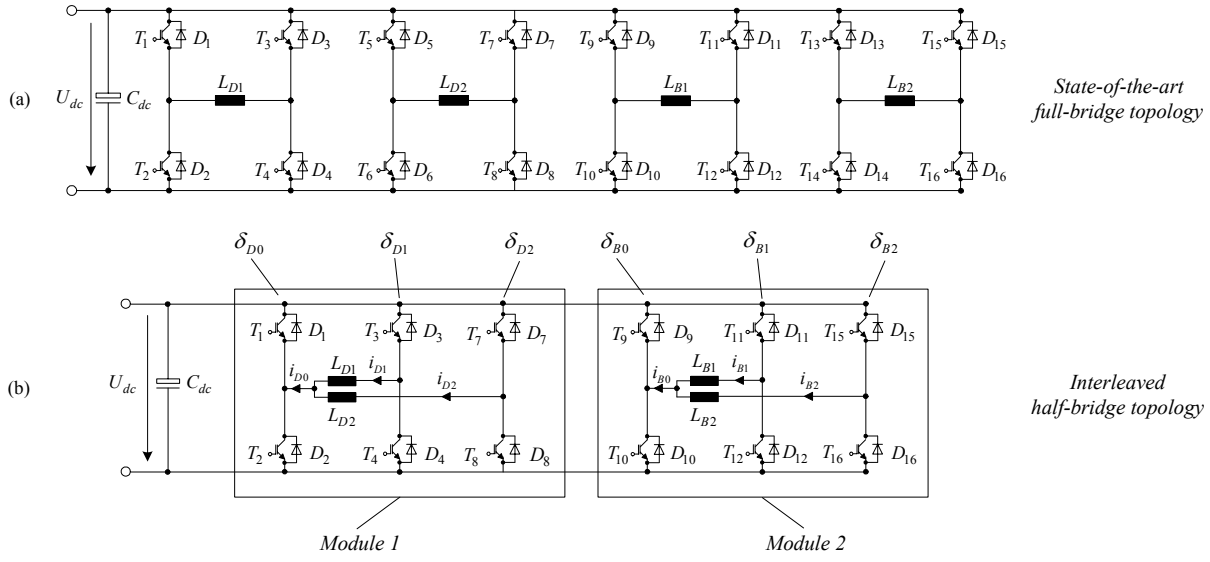

Fig. 1: Possible power electronic interfaces (a) State-of-the-art full-bridge topology for BSM for each drive (L_{Di}) and bearing (L_{Bi}) winding, (b) interleaved half-bridge topology with two common bridge legs for the two drive (L_{D1}, L_{D2}) and bearing (L_{B1}, L_{B2}) systems.

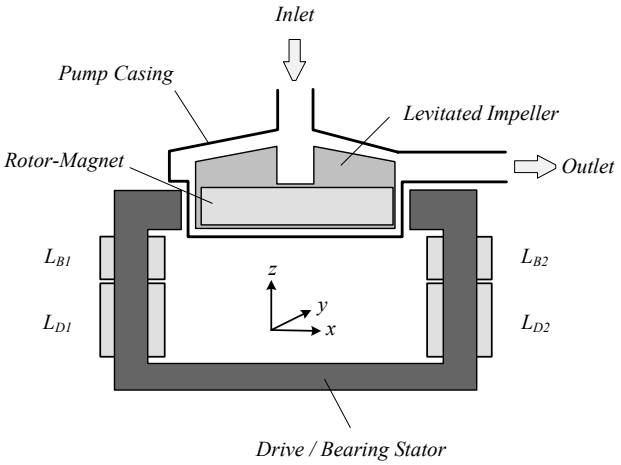

Fig. 2: Schematic of the basic principle of the bearingless centrifugal pump.

This paper presents and comparatively evaluates different modulation schemes for the interleaved half-bridge topology for the control of the BSM. First, the derivation of the interleaved half-bridge topology from the state-of-the-art full-bridge topology is briefly presented in **section II**. Starting with a constant common bridge leg modulation a more advanced modulation scheme with sinusoidally shaped common bridge leg duty cycles and an optimum phase shift between all bridge leg duty cycles is then derived in **section III**. In addition, the superposition of higher harmonics to the sinusoidally modulated duty cycles and their impact on the drive currents is presented. **Section IV** deals with the aspect of speed unbalances due to the before mentioned higher harmonics in the drive current and proves the theoretical considerations by measurements on a pump system. The maximum achievable drive power is then discussed in **section V** for the proposed modulation schemes. Finally, in **section VI**, the modulation schemes are verified by measurements on a 1.5kW prototype of the converter with a pump system.

II. Interleaved Half-Bridge Topology

In Fig. 1(a) the state-of-the-art converter topology for the control of the drive and bearing currents of the two-phase BSM is depicted. As described in detail in [3] the number of power semiconductors can be reduced if the power transistor/diode combinations T_5 /D_5 and T_6 /D_6 of the left bridge leg of the drive winding L_{D2} are removed. The two drive windings are now connected together with the junction of the bridge leg T_1 /D_1 and T_2 /D_2 (cf. Fig. 1(b)). This leg is used as the common bridge leg for the drive system. With this set-up the control of the drive system is realized by three interleaved half-bridges.

The same is done, in a similar way, with the two bearing windings. There, the combinations T_{13} /D_{13} and T_{14} /D_{14} are removed and the bearing windings are connected to the second common bridge leg consisting of the IGBTs and diodes T_9 /D_9 and T_{10} /D_{10}. This circuit allows a realization of the converter with only six power half-bridges, resulting in a total of twelve switches, by offering a similar control flexibility as the full-bridge converter as will be described in this paper later on. With the use of this interleaved half-bridge topology the total amount of switches needed to control the BSM is reduced by 25% compared to the state-of-the-art full bridge topology.

The idea of component minimization due to the connection of more than one motor winding to a common bridge leg has also been investigated in the area of the control of induction machines [5], [6]. There, a five-leg inverter is used to supply two three-phase induction machines. One leg of the five-leg inverter is simultaneously connected to both machines while the remaining inverter legs are connected to the two machines only. However, as it is the case for the before mentioned control of induction machines [7] new modulation schemes must be developed in order to achieve a similar performance and dynamical behaviour of the pump system as it is obtained with the standard full-bridge topology. Therefore, in the following section different modulation concepts are presented and evaluated comparatively.

III. Modulation Methods

In this section, different modulation methods for the interleaved half-bridge topology (cf. Fig. 1(b)) for the control of a BSM are analyzed. First, a basic modulation with lowest control effort is presented. Then, alternative modulation methods are characterized in order to provide higher modulation depth and therefore better motor performance.

The average voltages $\bar{u}_{D1}(t)$ and $\bar{u}_{D2}(t)$ of the drive coils are defined as

$$\begin{aligned} \bar{u}_{D1}(t) &= U_{dc} \cdot (\delta_{D1} - \delta_{D0}) = m \cdot U_{dc} \cdot \cos \omega t \\ \bar{u}_{D2}(t) &= U_{dc} \cdot (\delta_{D2} - \delta_{D0}) = m \cdot U_{dc} \cdot \sin \omega t, \end{aligned} \tag{1}$$

where the modulation depth m is defined as

$$m = \frac{\bar{u}_{\max}}{U_{dc}} = 0 \ldots m_{\max}, \tag{2}$$

with m_{max} = 0.95. This corresponds to the maximum value allowed to ensure a save operation of the system.

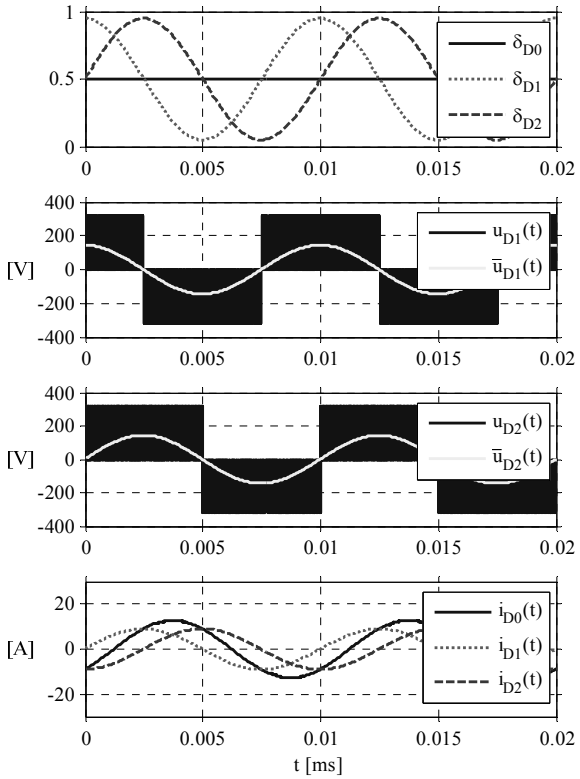

Fig. 3: Simulation results for constant common bridge leg modulation (CCM). Duty cycles δ_{D0}, δ_{D1} and δ_{D2}, switched voltage u_{D1} and average voltage $\bar{u}_{D1}$ across coil L_{D1}, switched voltage u_{D2} and average voltage $\bar{u}_{D2}$ across coil L_{D2} and currents i_{D0}, i_{D1} and i_{D2} of the drive system.

Moreover, U_{dc} stands for the dc-link voltage and δ_{D0}, δ_{D1} and δ_{D2} are the duty cycles applied to the upper switches in each bridge leg of the drive module [cf. Fig. 1(b)]. The duty cylces of the lower switches are then given by (1-δ_{Di}) with i=1,2,3. In the following, only the expression δ_{Di} is used to describe the duty cycles of the bridge legs. Furthermore, $\bar{u}_{max}$ is the maximum value of the average voltage (local average value over one pulse period) at the junction point of a bridge leg. Analogously, the duty cycles δ_{B0}, δ_{B1} and δ_{B2} are applied to the upper switches of the bearing module in Fig. 1(b). The operation of the interleaved half bridge converter is done with unipolar modulation as it is described in [8].

Due to the fact, that the major part of the power consumption is taken by the drive system the requirements regarding the modulation range are higher for the drive part. Hence, in the following different modulation concepts are discussed for the drive system. However, the considerations are also valid for the modulation of the bearing currents.

A. Constant Common Bridge Leg Modulation (CCM)

In this basic modulation scheme the duty cycle δ_{D0} of the common bridge leg is kept constant at δ_{D0} = 0.5. This leads to an average potential of U_{dc} /2 at the connection point of the two windings. In addition, the duty cycles δ_{D1} and δ_{D2} are sinusoidally modulated with

$$\begin{aligned}\delta_{D1} &= \frac{1}{2}+\frac{m}{2}\cos(\omega t)\\ \delta_{D2} &= \frac{1}{2}+\frac{m}{2}\sin(\omega t).\end{aligned} \tag{3}$$

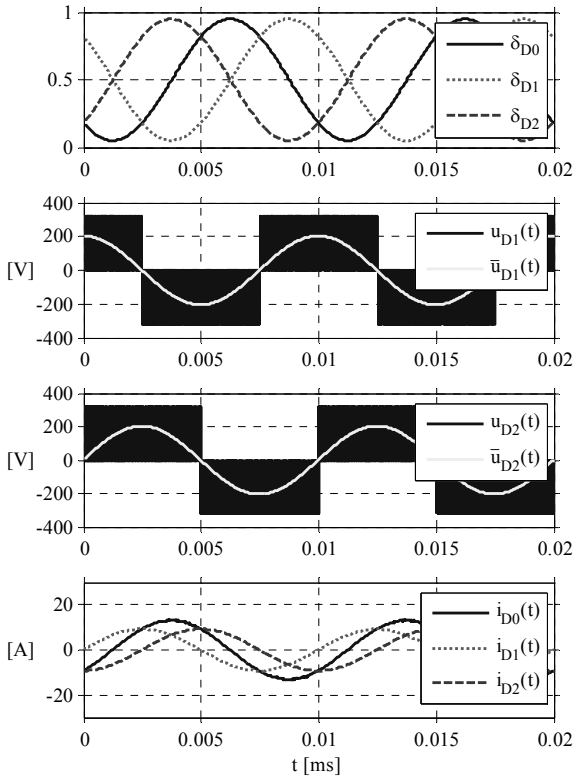

Fig. 4: Simulation results for sinusoidal common bridge leg modulation (SCM). Duty cycles δ_{D0}, δ_{D1} and δ_{D2}, switched voltage u_{D1} and average voltage $\bar{u}_{D1}$ across coil L_{D1}, switched voltage u_{D2} and average voltage $\bar{u}_{D2}$ across coil L_{D2} and currents i_{D0}, i_{D1} and i_{D2} of the drive system.

This can be seen in **Fig. 3**. Furthermore, the resulting voltages $\bar{u}_{D1}(t)$ and $\bar{u}_{D2}(t)$

$$\begin{aligned}\bar{u}_{D1}(t) &= \frac{m}{2}\cdot U_{dc}\cdot\cos\omega t\\ \bar{u}_{D2}(t) &= \frac{m}{2}\cdot U_{dc}\cdot\sin\omega t,\end{aligned} \tag{4}$$

and currents $i_{D0}(t)$, $i_{D1}(t)$ and $i_{D2}(t)$ of the two drive windings are depicted in Fig. 3 as well. It can be seen that the maximum average voltage across a drive coil obtainable with the described modulation scheme is given by:

$$\bar{u}_{D\max} = m_{\max}\cdot\frac{U_{dc}}{2}. \tag{5}$$

Compared to the conventional modulation of the full-bridge topology (cf. Fig. 1(a)) this voltage is therefore reduced by a factor 2. Especially for the drive system, where high voltages across the coils are needed in order to deliver high pump power, this performance decrease can be unacceptable. Therefore, in the following different modulation schemes are developed which provide higher modulation ratios as the one obtained with CCM.

B. Sinusoidal Common Bridge Leg Modulation (SCM)

An increased modulation ratio is achievable for the drive system if the duty cycle δ_{D0} of the power switch T_1 (cf. Fig. 1(b)) in the common bridge leg is varied sinusoidally. For the calculation of the required duty cycle we assume that the gate signals of all switches are phase shifted by the angle φ_0

$$\delta_{D0} = \frac{1}{2}+\frac{m}{2}\sin(\omega t+\varphi_0), \tag{6}$$

and that δ_{D1} and δ_{D2} are symmetrically distributed with respect to δ_{D0} by the angle $\Delta\varphi$:

$$\begin{aligned}\delta_{D1} &= \frac{1}{2}+\frac{m}{2}\sin(\omega t+\varphi_0-\Delta\varphi)\\ \delta_{D2} &= \frac{1}{2}+\frac{m}{2}\sin(\omega t+\varphi_0+\Delta\varphi).\end{aligned} \tag{7}$$

A symmetrical distribution of δ_{D1} and δ_{D2} to ωt is chosen due to the fact that the same modulation depth for both drive windings is desired.

In the following, the calculation of the optimal values of φ_0 and $\Delta\varphi$ for highest modulation depth is presented. Combining (1), (6) and (7) results in the following expression for $\bar{u}_{D1}(t)$

$$\bar{u}_{D1}(t) = m\cdot U_{dc}\cos(\omega t+\varphi_0-\frac{\Delta\varphi}{2})\sin(-\frac{\Delta\varphi}{2}) \overset{!}{=} \hat{U}\cos\omega t. \tag{8}$$

Analogously $\bar{u}_{D2}(t)$ can be calculated to:

$$\bar{u}_{D2}(t) = m\cdot U_{dc}\cos(\omega t+\varphi_0+\frac{\Delta\varphi}{2})\sin(\frac{\Delta\varphi}{2}) \overset{!}{=} \hat{U}\sin\omega t. \tag{9}$$

Solving (7) and (8) for φ_0 and $\Delta\varphi$ leads to

$$\begin{aligned}\varphi_0 &= -\frac{3\pi}{4}\\ \Delta\varphi &= \frac{\pi}{2},\end{aligned} \tag{10}$$

and therefore to the following expressions for δ_{D0}, δ_{D1} and δ_{D2}:

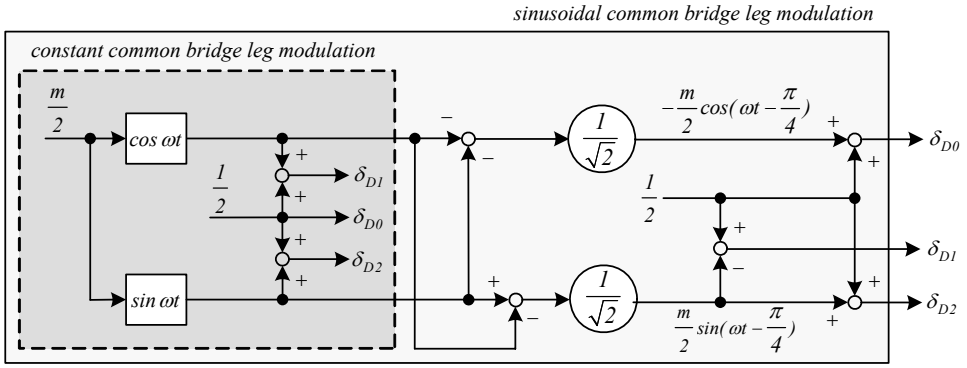

Fig. 5: Analog implementation of the sinusoidal common bridge leg modulation with resulting duty cycles δ_{D0}, δ_{D1} and δ_{D2}.

$$\begin{aligned}\delta_{D0} &= \frac{1}{2}+\frac{m}{2}\sin(\omega t-\frac{3\pi}{4}) = \frac{1}{2}-\frac{m}{2}\cos(\omega t-\frac{\pi}{4})\\ \delta_{D1} &= \frac{1}{2}+\frac{m}{2}\sin(\omega t-\frac{5\pi}{4}) = \frac{1}{2}-\frac{m}{2}\sin(\omega t-\frac{\pi}{4})\\ \delta_{D2} &= \frac{1}{2}+\frac{m}{2}\sin(\omega t-\frac{\pi}{4}) = \frac{1}{2}+\frac{m}{2}\sin(\omega t-\frac{\pi}{4}),\end{aligned} \tag{11}$$

and for $\bar{u}_{D1}(t)$ and $\bar{u}_{D2}(t)$:

$$\begin{aligned}\bar{u}_{D1}(t) &= \frac{m}{\sqrt{2}}\cdot U_{dc}\cdot\cos\omega t\\ \bar{u}_{D2}(t) &= \frac{m}{\sqrt{2}}\cdot U_{dc}\cdot\sin\omega t.\end{aligned} \tag{12}$$

With this, the new duty cycles δ_{D1} and δ_{D2} are phase shifted by π while the angle between the winding currents $i_{D1}(t)$ and $i_{D2}(t)$ remains $\pi/2$ (cf. **Fig. 4**). As can be seen in (12), the voltages across the drive coils achievable with the SCM scheme are increased by a factor of $\sqrt{2}$ (= +41%) as compared to the CCM method.

In **Fig. 5** it is shown how the duty cycles δ_{D0}, δ_{D1} and δ_{D2} of the SCM method can be calculated out of the duty cycles δ_{D0}, δ_{D1} and δ_{D2} of the CCM method by an analog implementation.

C. Harmonic Injection

Following the concept of the SCM (section III.B) additional higher harmonics can be superposed to the common bridge leg duty cycle in order to further increase the modulation depth. In a first approach a third harmonic is superposed to a purely sinusoidally shaped duty cycle. This provides a higher utilization of the dc bus voltage. The amount of the third harmonic and the fundamental component is chosen so that the latter is maximized while ensuring that the peak-to-peak amplitude does not exceed the maximum allowed modulation depth. The corresponding average duty cycle is depicted in **Fig. 6**(b). With this, the voltage-time product is increased compared to purely sinusoidal modulation. Adding additional higher harmonics to the sinusoidal fundamental subsequently leads to a full square wave as it can be seen in the waveform Fig. 6(d).

Different from the before discussed modulation schemes the duty cycle can be limited to the maximum applicable modulation depth over a certain amount of time (e.g. 120°) while it is increasing/decreasing at the beginning/end of a half period (Fig. 6(c)). However, this does not lead to a significant increase of the first harmonic amplitude of the voltages applied to the drive coils compared to third harmonic modulation and thus will not be investigated in the following.

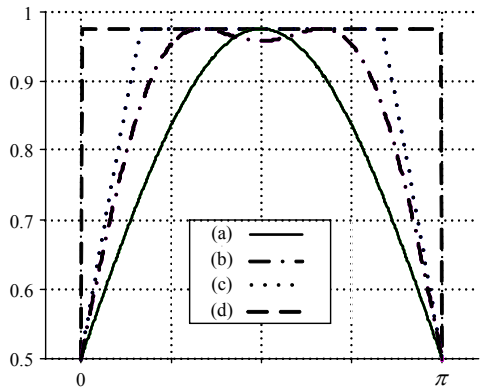

Fig. 6: Duty cycle waveform for (a) purely sinusoidal, (b) third harmonic, (c) constant 120° and (d) full square wave modulation.

C.1. Third Harmonic Modulation (THM)

Applying the previously discussed concept of the superposition of a third harmonic to each of the duty cycles, while keeping the same phase shift as it is defined for SCM, leads to another modulation concept denominated as third harmonic modulation (THM). The resulting duty cycles δ_{D0}, δ_{D1} and δ_{D2} of the three half bridges are:

$$\begin{aligned}\delta_{D0} &= \frac{1}{2}-\frac{m}{\sqrt{3}}\cos(\omega t-\frac{\pi}{4})+\frac{m}{6\sqrt{3}}\cos(3\omega t-\frac{3\pi}{4})\\ \delta_{D1} &= \frac{1}{2}-\frac{m}{\sqrt{3}}\sin(\omega t-\frac{\pi}{4})+\frac{m}{6\sqrt{3}}\sin(3\omega t+\frac{\pi}{4})\\ \delta_{D2} &= \frac{1}{2}+\frac{m}{\sqrt{3}}\sin(\omega t-\frac{\pi}{4})-\frac{m}{6\sqrt{3}}\sin(3\omega t+\frac{\pi}{4}).\end{aligned} \tag{13}$$

The duty cycle, voltage and current waveforms for the THM method are shown in **Fig. 7**(a). Compared to CCM the first harmonic of the drive voltage is increased by a factor of $2\sqrt{2}/\sqrt{3}$ (= +63%). A drawback of this control technique clearly is that the currents in the windings are not sinusoidal anymore. This issue will be further investigated in section IV.

C.2. Square Common Bridge Leg Modulation (QCM)

Unlike the previously presented modulation schemes for the QCM the duty cycle of the common bridge leg δ_{D0} is of rectangular shape (cf. Fig. 7(b)) with the same phase shift φ_0 as it has been used for THM and SCM. This modulation of the common bridge leg represents the maximum quantity of superposed higher harmonics which leads to a full square wave. The average duty cycles δ_{D1} and δ_{D2} are sinusoidally

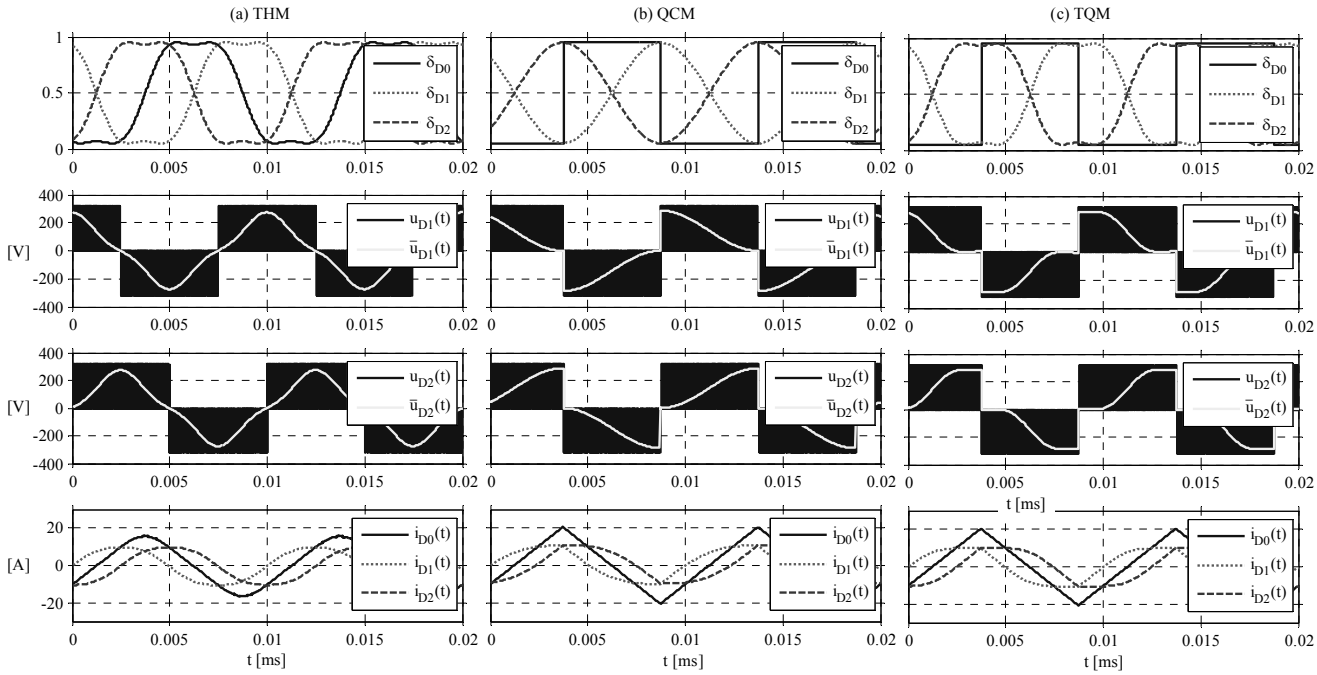

Fig. 7: Simulation results for (a) THM, (b) QCM and (c) TQM with duty cycles δ_{D0}, $\delta_{D1}$and δ_{D2}, switched voltage u_{D1} and average voltage $\bar{u}_{D1}$ across coil L_{D1}, switched voltage u_{D2} and average voltage $\bar{u}_{D2}$ across coil L_{D2} and currents i_{D0}, i_{D1} and i_{D2} of the drive system.

modulated and show a phase shift of $\pi/2$. The maximum amplitude of the fundamental harmonic of the applied drive voltage is increased by 62% compared to the one achieved with CCM.

C.3. Third Harmonic & Square Common Bridge Leg Modulation (TQM)

A further increase in the maximum current amplitude can be achieved when combining the idea of the THM and the QCM. This leads to a square wave modulation of the duty cycle in the common bridge δ_{D0} while superposing third harmonics to the sinusoidal fundamental of the duty cycles δ_{D1} and δ_{D2} as it is depicted in Fig. 7(c). With this modulation scheme the fundamental drive voltage is increased by 72% compared to CCM.

D. Comparison of Modulation Schemes

In order to compare the effect of the presented modulation schemes the fundamental harmonic of the voltage applied to the drive coil L_D is calculated for each of the average voltages $\bar{u}_{D1}(t)$ depicted in Fig. 3, 4 and 7.

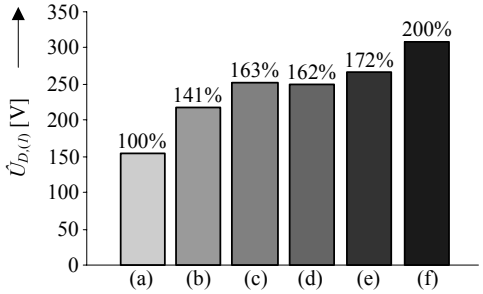

Fig. 8: Maximum applicable fundamental amplitude of drive voltage $u_{D(1)}$ achieved with the (a) CCM (b) SCM (c) QCM (d) THM (e) TQM and (f) FBM method.

The comparison is done with the value obtained with the state-of-the-art full-bridge modulation method (FBM) implemented for the control of the topology in Fig. 1(a).

As can be seen in **Fig. 8** is the maximum amplitude achievable with the CCM method half of that which results from FBM. Furthermore, the maximum voltage that can be obtained with the optimal modulation scheme (TQM) for the interleaved half-bridge topology is 86% of that resulting with FBM and the state-of-the-art full-bridge topology (cf. Fig. 1(b)).

IV. Analysis of Speed Oscillations due to Harmonic Injection

In the previous sections, starting from the purely sinusoidal modulation concepts (CCM, SCM), gradually higher harmonics have been superposed in order to increase the modulation depth. However, as already stated before, this results in progressively more distorted current waveforms.

In this paragraph, it shall be investigated to which extent this higher harmonic distortion takes influence on speed oscillations in the pump system which then result in higher vibrations of the impeller which limits it lifetime. Latter is a known issue in not only the design of bearingless but also in the design of conventional pumps [9].

In a first step, a reference operating point of the pump and the motor is chosen under steady state conditions where the impeller is held at constant angular speed of ω_0. Furthermore, the pump is working against a given load $P_{hydr} = P_0$. The average torque M_0 that is exerted by the average torque current $\bar{i}_{q0}$ on the impeller is in equilibrium with all dynamic and frictional forces:

$$M_0 = c_m \bar{i}_{q0}. \tag{14}$$

Here, c_m is the torque constant of the motor.

The time-dependent worst case torque generating current component through all drive coils $i_q(t)$ is represented by a square wave function with an amplitude Δi_q around the average value of $\bar{i}_{q0}$ as it is shown in **Fig. 9**. Since the torque exerted on the rotor is strictly proportional to the drive current, it is also represented by a square wave function within the range $M_0 - \Delta M \le M(t) \le M_0 + \Delta M$, where

$$\Delta M = c_M \cdot \Delta i_q. \tag{15}$$

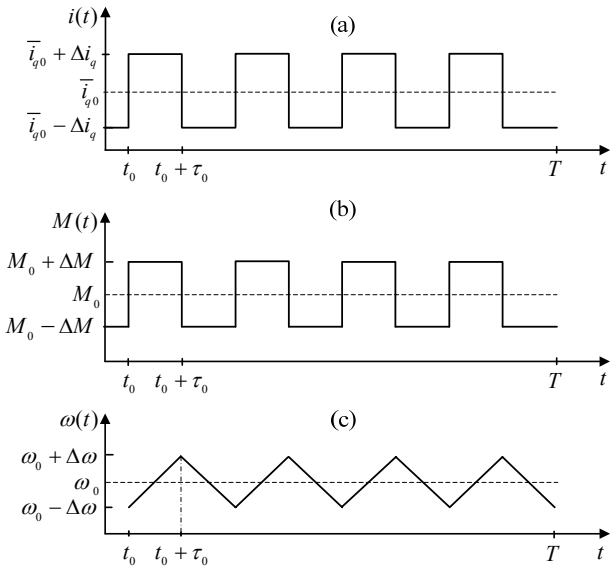

Fig. 9: Estimated worst case current waveform of the torque generating current $i_q(t)$, the resulting torque $M(t)$ and the subsequent speed $\omega(t)$ of the motor.

With this, the worst case speed oscillation occurs where the speed oscillates around an average value of ω_0. The characteristic time scale of this square-wave function is τ_0, which corresponds to the length of one period of the ideally sinusoidal drive current divided by twice the number of drive coils n_{drc}:

$$\tau_0 = \frac{2\pi}{\omega_0} \cdot \frac{1}{2n_{drc}}. \tag{16}$$

Each of the two drive windings L_{D1} and L_{D2} (cf. **Fig. 1**(b)) is built up with two coils connected in series. Thus, the number of drive coils arranged over one full circle is $n_{drc} = 4$.

A cut-off frequency ω_0 is then defined by applying a criterion according to which the time scale of this square-wave function must be smaller than a typical acceleration time of the impeller resulting from the torque characteristic given with:

$$\tau_{acc} = \frac{1}{\xi_0} \cdot \frac{\omega_0 \cdot J}{c_m \cdot \bar{i}_{q0}} > \tau_0, \tag{17}$$

where ξ_0 is a dimensionless system specific constant.

Implementing (16) into (17) and resolving the latter for ω_0 leads to

$$\omega_0 > \sqrt{\pi\xi_0} \cdot \tilde{\omega}, \tag{18}$$

where

$$\tilde{\omega} = \sqrt{\frac{c_m \cdot \bar{i}_{q0}}{n_{drc} \cdot J}}. \tag{19}$$

The motor investigated here has a torque constant c_m = 0.282Vs. With a reference current of $\bar{i}_{q0}$ = 4A and an estimated geometrical moment of inertia of J = 300 kgmm^2, and $\pi\xi_0$ = 6.28 for the used motor the reference frequency in (19) can be determined as ω = 76.83 rad/s. This result translates into a cut-off pump speed of

$$\frac{60}{2\pi} \cdot \frac{s}{\min} \cdot \omega_0 = n_0 > 734 rpm. \tag{20}$$

Above this speed, the effects of higher harmonic components of the drive current on the evenness of the angular speed of the impeller are presumably attenuated significantly.

Experiments with the pump driven in single-phase operation under load have shown that at a speed of n = 5000rpm, above that the pump is operating with a reasonable hydraulic power, the induced voltage $u_{ind}(t)$ measured across the open coil is purely sinusoidal as can be seen in **Fig. 10** although the current is obviously distorted significantly. This leads to the conclusion that the impeller is rotating at constant speed despite of higher harmonics superposed to the drive current. This current waveform is obtained with the modulation scheme presented in section III.C.3 (TQM).

Due to these considerations it has been proven that the impeller speed of the pump can be assumed to be constant. This implicates a non pulsating and thus constant output flow of the pump.

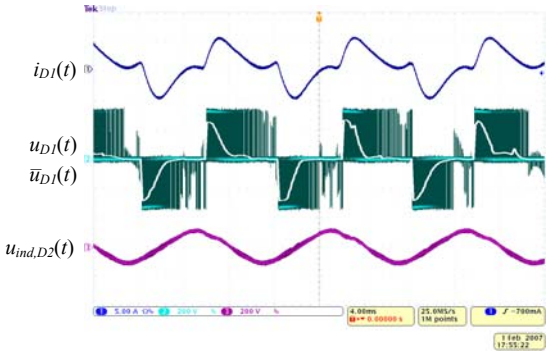

Fig. 10: Experimental results for the induced voltage for highly distorted drive currents obtained with TQM. Time behavior of drive current i_{D1}, switched voltage u_{D1} and average voltage $\bar{u}_{D1}$ across drive coil L_{D1} and induced voltage $u_{ind,D2}$ in drive L_{D2}. Current scale: i_{D1}: 5A/div, voltage scale: u_{D1}, $u_{ind,D2}$: 200V/div, time scale: 4ms/div.

V. Maximum Achievable Drive Power

The maximum applicable drive power to each of the two motor phases is depending on the induced voltage $\hat{u}_{ind}$ and the current $\hat{i}_{D(1)}$, which is in phase with $\hat{u}_{ind}$ for the field oriented control (cf. **Fig. 11**), flowing through that drive coil.

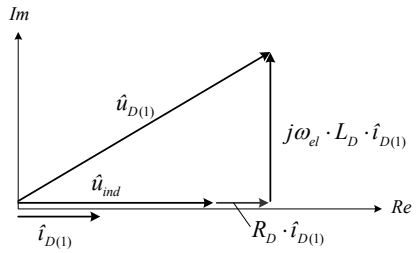

Fig. 11: Phasor chart of the equivalent electrical circuit of one drive phase with the basic phasor orientation.

Due to the fact, that the induced voltage does not contain higher harmonics (see section IV), only the fundamental harmonic of that current needs to be considered for the calculation of the drive power.

Doing this, leads to the following equation for the motor drive power P_D of one drive winding:

$$P_D = u_{ind,rms} \cdot i_{D,(1),rms}, \tag{21}$$

where $i_{D,(1),rms}$ is the rms value of the fundamental harmonic of the current in the drive phase one and $u_{ind,rms}$ is the rms value of the induced voltage in that winding, which is experimentally measured to $u_{ind,rms}$ = 15.8V/1000rpm for the here employed motor.

According to the phasor chart shown in Fig. 11, the following equation is given:

$$\left(\hat{u}_{ind} + R_D \cdot \hat{\imath}_{D(1)}\right)^2 + \left(\omega_{el} \cdot L_D \cdot \hat{\imath}_{D(1)}\right)^2 = \hat{u}^2_{D(1)}, \tag{22}$$

where ω_{el} is the rotating speed of the impeller in rad/s.

Solving (30) for $\hat{\imath}_{D1}$ results in:

$$\hat{\imath}_{D(1)} = \frac{-\hat{u}_{ind} \cdot R_D \pm \sqrt{\left(R_D{}^2 + \omega_{el}{}^2 \cdot L_D{}^2\right) \cdot \hat{u}^2_{D(1)} - \omega_{el}{}^2 \cdot L_D{}^2 \cdot \hat{u}^2_{ind}}}{R_D{}^2 + \omega_{el}{}^2 \cdot L_D{}^2} \tag{23}$$

With (21) and (23) the total drive power of the two drive phases can now be calculated for different rotating speeds. In **Fig. 12** the maximal achievable drive power depending on the chosen modulation scheme is shown for U_{dc} = 320V, m_{max} = 0.95 and $I_{D,max,rms}$ = 10A. There, the methods that have been presented in section III are compared to the state-of-the-art full-bridge modulation (FBM) operated with the topology in Fig. 1(a). For these calculations a motor with an inductance L_D = 35mH and R_D = 720mΩ per drive phase is employed.

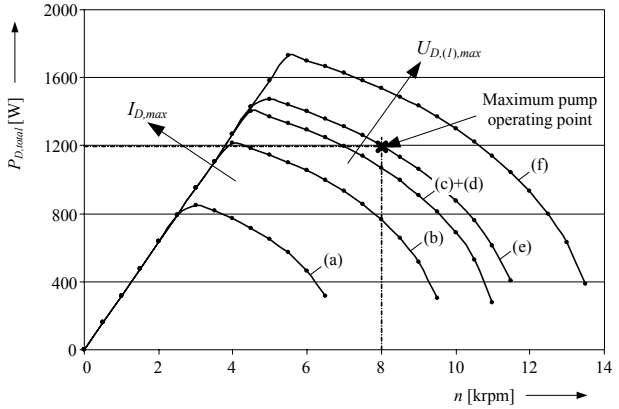

Fig. 12: Total achievable drive power for the motor with (a) CCM (b) SCM (c) QCM (d) THM (e) TQM and (f) FBM method.

As can be seen in **Fig. 12**, above rotating speed of 6500rpm the CCM method cannot be utilized anymore since the induced voltage is becoming higher than the maximum applicable voltage, whereas with SCM still three times the power can be delivered to the drive system at this speed. The power rating can be further improved when switching to an increased modulation depth by using the QCM, THM (which have the same performance) or finally the TQM method.

The maximum hydraulic power of the pump is limited to a flow of 100l/min with a pressure of 3.6bar [10]. This is achieved at a speed of n = 8000rpm and the necessary drive power required to operate the pump at this point is 1190W. According to Fig. 12 this can be achieved by the TQM method with no performance decrease compared to the conventional full-bridge topology with its modulation. Furthermore, it can be seen that the achievable drive power is limited for lower rotational speeds by the maximum allowable drive current. On the other hand, for higher speeds the maximum applicable drive voltage that is ensured by the respective modulation scheme limits the achievable drive power.

VI. Experimental Verification

The proposed modulation schemes have been implemented on a DSP and tested with a prototype (cf. **Fig. 13**) of a 1.5kW converter. This system is built up with two integrated half-bridge power modules [11] for the drive and bearing system and is operated from a single phase mains voltage. Each IGBT of these modules has a maximum peak current rating of 30A. The switching frequency of the drive and bearing system is chosen to 17.5kHz.

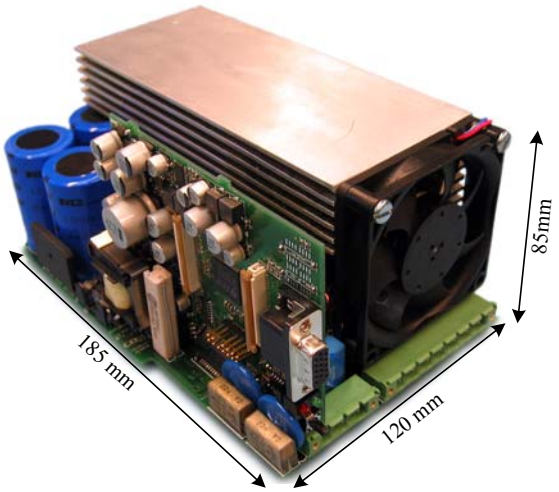

Fig. 13: Prototype of the 1.5kW interleaved half-bridge converter with two integrated three phase power modules for the control of the drive and bearing system.

A. Verification of modulation schemes

In **Fig. 14**, the current and voltage waveforms in the drive system generated by the different modulation schemes are presented. The measured shapes of the drive currents i_{D1} and i_{D2} are in good agreement with the simulation results (cf. Fig. 3, 4 and 7).

Furthermore, tests with a bearingless pump system under load have been carried out in order to show the resulting maximum torque limits of the different modulation schemes. As an example, the result for the THM method is presented in **Fig. 15**. This allows it to rotate the impeller with a speed of 8500rpm while regulating the flow to 38l/min. The resulting output pressure is then 4.5bar. The current i_{B1} in the bearing phase L_{B1}, the drive current i_{D1}; the common bridge leg current i_{D0}, as well as the switched voltage u_{D1} across the drive coil L_{D1} are shown in the aforesaid figure. As can be seen, the bearing current i_{B1} depicted in that figure is relatively small compared to the drive current i_{D1} and thus the CCM method is sufficient to control that current.

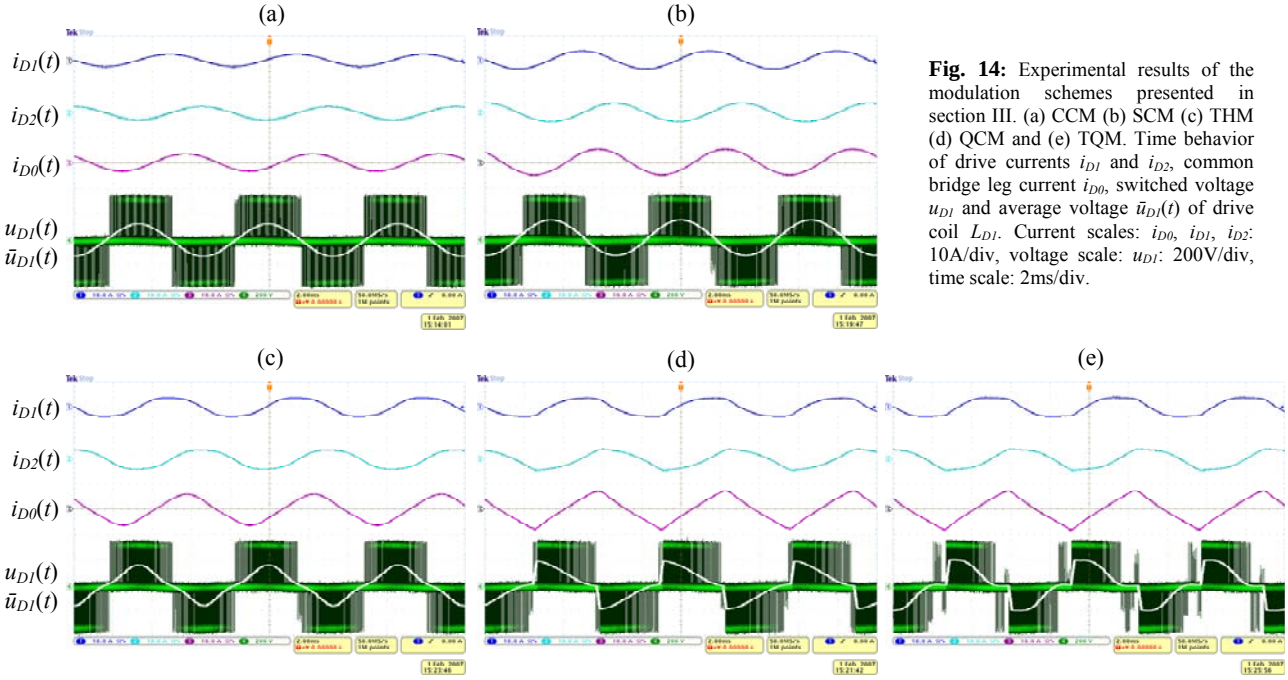

Fig. 14: Experimental results of the modulation schemes presented in section III. (a) CCM (b) SCM (c) THM (d) QCM and (e) TQM. Time behavior of drive currents i_{D1} and i_{D2}, common bridge leg current i_{D0}, switched voltage u_{D1} and average voltage $\bar{u}_{D1}(t)$ of drive coil L_{D1}. Current scales: i_{D0}, i_{D1}, i_{D2}: 10A/div, voltage scale: u_{D1}: 200V/div, time scale: 2ms/div.

Thus, the control of the bearing system with the CCM method still ensures a sufficient performance over the whole operating range of the pump, while for the control of the drive system for higher power and/or rotation speeds the presented more advanced modulation techniques have to be employed (cf. Fig. 12). E. g. the shown operating point in Fig. 15 could not be achieved by the CCM or SCM method.

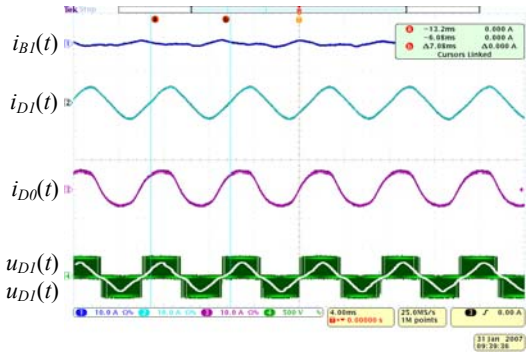

Fig. 15: Experimental results for the pump under operation employing the THM method with an impeller speed of 8500rpm, a flow of 38.5l/min and resulting pressure of 4.5bar. Time behavior of bearing current i_{B1}, drive current i_{D1}, common bridge leg current i_{D0}, switched voltage u_{D1} and average voltage across $\bar{u}_{D1}(t)$ of drive L_{D1}. Current scales: i_{B1}, i_{D1}, i_{D0}: 10A/div, voltage scale: u_{D1}: 500V/div, time scale: 4ms/div.

VII. Summary

In this paper, novel modulation concepts for the control of a two-phase bearingless slice motor pump operated with the interleaved half-bridge topology are presented. Starting with a constant common bridge leg modulation more advanced modulation concepts with the superposition of higher harmonics are then presented. The proposed modulation schemes are compared based on the maximum achievable drive power for the motor. With the highest level of harmonic superposition the maximum voltage applicable to the drive phases is 86% of that obtained with the state-of-the-art full-bridge topology and its control method. As shown in analytical calculations these higher harmonics in the drive current do not have an impact on the constant speed of the impeller and thus on the constant output flow of the pump. This is finally verified by measurements on a pump system with a 1.5kW converter realized with integrated half-bridge power modules.

VIII. References

[1] R. Schöb, "The Future in Hand – A New Type of Pump for Delicate Fluids", World Pumps, Number 430, July 2002.

[2] J. Bichsel, "Beiträge zum lagerlosen Elektromotor", Ph.D. Dissertation, Electrical Engineering and Design Laboratory, ETH Zurich, 1990.

[3] M. Neff, N. Barletta, R. Schöb, "Magnetically levitated centrifugal pump for highly pure and aggressive chemicals", PCIM Conference 2000, June 6-8, 2000, Nuremberg, Germany.

[4] M.T. Bartholet, T. Nussbaumer, P. Dirnberger, J.W. Kolar, "Novel Converter Concept for Bearingless Slice Motor Systems", IEEE Industry Applications Conference 2006, Conference Record of the 41st IAS Annual Meeting, October 2006, Tampa, USA, vol. 5, pp. 2496-2502.

[5] B. Francois, A. Bouscayrol, "Design and modelling of a five-phase voltage-source inverter for two induction motors", Proc. Eur. Conf. on Power Elec. and Appl. EPE, Lausanne, Switzerland, 1999, CD-ROM paper 626.

[6] C.B. Jacobina, T.M. Oliveira, M.B. de R. Correa, A.M.N. Lima, E.R.C. da SILVA, "Component minimized drive systems for multimachine applications", Proc. IEEE Power Elec. Spec. Conf. PESC, 2002, Cairns, Australia, CD-ROM paper 10028.

[7] Ph. Delarue, A. Bouscayrol, B. Francois, Control implementation of a five-leg voltage-source-inverter supplying two three-phase induction machines, *Proc. IEEE Int. Elec. Mach. & Drives Conf. IEMDC*, 2001, Madison, USA, pp. 1909-1915.

[8] N. Mohan, T.M. Undeland, W.P. Robbins, *"Power Electronics: Converters, Applications and Design."* 2nd Edition, 1995, New York: John Wiley&Sons.

[9] Sulzer Pumps, Sulzer *Centrifugal Pump Handbook*, 2nd ed. Oxford, UK: Elsevier Advanced Technology, 1998.

[10] Levitronix Pumps: http://www.levitronix.com

[11] International Rectifier: Integrated Hybrid IC IRAMY30UP60B, Datasheet (2006).